This is a non-peer-reviewed manuscript submitted to EarthArxiv. The manuscript was submitted for review to Geophysical Research letters.

Using thermal springs to quantify deep groundwater flow and its thermal footprint in the Alps and North American orogens

Elco Luijendijk[1], Theis Winter[1,2], Saskia Köhler[1,3], Grant Ferguson[4], Christoph von Hagke[5], Jacek Scibek[6]

[1]Department of structural geology & geodynamics, University of Göttingen, Goldschmidtstrasse 3, 37077, Göttingen, Germany

[2]Chair of Hydrogeology, Faculty of Civil, Geo and Environmental Engineering, Technical University of Munich, Arcisstr. 21, 80333 Munich, Germany

[3]GeoZentrum Nordbayern, Universität Erlangen-Nürnberg, Schlossgarten 5, 91054 Erlangen, Germany

[4]Department of Civil, Geological and Environmental Engineering, University of Saskatchewan, 57 Campus Drive, Saskatoon, Canada

[5]Geological Institute of the RWTH Aachen University, Wüllnerstr. 2, 52056 Aachen, Germany.

[6]No fixed address at present (travelling through Japan)

Corresponding author: Elco Luijendijk (elco.luijendijk@geo.uni-goettingen.de)

Key Points:

- Thermal springs in the Alps are exclusively fed by meteoric water which on average circulates to a depth of at least 2100 m
- On average the contributing area of springs is 0.6 km^2 and the thermal footprint is 6 km^2
- The magnitude of cooling by downward flow and heating by upward flow equals ~6.5% and ~5.0% of the background heat flow, respectively

Abstract

The extent of deep groundwater flow in mountain belts and its thermal effects are uncertain. Here, we use a new database of discharge, temperature and composition of thermal springs in the Alps to estimate the extent of deep groundwater flow and its contribution to the groundwater and heat budget. The results indicate that springs are fed exclusively by meteoric water and make up 0.13% of the total groundwater budget. Spring water circulates on average to a depth of at least 2100 m. The net heat extracted from the subsurface equals 1.5% of the background heat flow, which equals an average thermal footprint for springs of 6 km^2. Cooling by downward flow and heating by upward flow are estimated as approximately 6.5% and 5.0% of the background heat flow, respectively. Compared to orogens in North America the Alps have a relatively high amount of hydrothermal activity.

Plain Language Summary

Groundwater that originates as rainfall may reach considerable depths in mountain belts. Groundwater can also transport heat and affect the heat budget of mountains. However, the amount of groundwater that circulates to deeper levels and the extent to which it affects subsurface temperatures is largely unknown. Here we analyze newly compiled data from hot springs in the Alps to quantify groundwater flow and its thermal effects. On average the groundwater discharging in springs reach a depth of at least 2100 m. The thermal spring water makes up a very small portion (0.13%) of all the groundwater in the Alps, while almost all of the groundwater flows out into rivers and lakes or evaporates. However, the groundwater that feeds springs does affect temperatures of rocks considerably. During downward flow it cools the subsurface, and during upward flow it heats the subsurface.

1 Introduction

Deep groundwater flow in mountains belts affects fault strength (Hubbert & Rubey, 1959; Wintsch et al., 1995), subsurface temperatures and heat flow (Bodri & Rybach, 1998; Whipp & Ehlers, 2007). Moreover, groundwater flow may connect the deep and shallow biospheres (Pedersen, 1993; Walvoord et al., 1999). Groundwater can penetrate large parts of the crust, as shown by stable isotopes of fault minerals (Person et al., 2007; Poulet et al., 2014) and elevated $^3He/^4He$ ratios in thermal springs (Hoke et al., 2000; Karlstrom et al., 2013; Umeda et al., 2007). However, in contrast to sedimentary basins, where borehole data has yielded information on the volume, composition and age of deep groundwater (Ferguson et al., 2018; Gleeson et al., 2016; Jasechko et al., 2017), the overall rate and extent of deep groundwater flow in orogens is largely unknown. Note that we define deep groundwater as groundwater at depths exceeding 200 m, following the approximate lower boundary of the hydrologically active zone in orogens (Manning & Caine, 2007).

Several studies have shown that groundwater flow can influence temperatures in orogens by tens of degrees (Bodri & Rybach, 1998; Forster & Smith, 1989; Maréchal et al., 1999). The extent of the thermal effects of groundwater flow has been a long-standing question, in particular in low-temperature thermochronology, where anomalous thermochronological ages are often the

result of hydrothermal activity (Dempster & Persano, 2006; Duddy et al., 1994; Louis et al., 2019). Models and data from thermal springs have suggested that in some regions in the Himalayas (Derry et al., 2009; Whipp & Ehlers, 2007) or the Cascades (Ingebritsen et al., 1992) groundwater flow may be responsible for more than 50% of the heat transport. Yet, the overall contribution of groundwater flow to the heat budget of orogens has not been quantified systematically to our knowledge.

Thermal springs are the most visible surface expression of deep groundwater flow in orogens. Data on spring discharge and temperature offers opportunities to quantify deep groundwater flow and its thermal effects (Luijendijk, 2019; Manga, 2001). The only systematic compilation and analysis of thermal springs in orogens known to us covers North America (Ferguson & Grasby, 2011). However, this study did not report the contribution of thermal springs to the groundwater and heat budget of orogens. Country-wide estimates of spring discharge and heat flow exist for Japan (Fukutomi, 1970; Sumi, 1980), but these include a large number of pumping wells in addition to natural springs. Here, we report a new database of thermal springs in the Alps that includes temperature, discharge, hydrochemistry and isotope data. We use this database to quantify groundwater origin, circulation depth and the contribution of thermal springs to the groundwater and heat budget of the Alps. In addition, we compare the results to published data for orogens in North America.

2 Methods

Our database contains data for 394 thermal springs in the Alps, including temperature, discharge, hydrochemistry (pH, TDS, major ions, SiO_2) and stable isotopes (^{18}O, ^{2}H). The dataset predominantly consists of natural springs, but also includes 32 springs that are tapped by wells that are less than 100 m deep. A description of the data compilation methods and spring sites can be found in the supporting information S1. The dataset is available on Pangaea (DOI to be supplied).

The origin of spring water was assessed by comparing the $\delta^{18}O$ and $\delta^{2}H$ values in thermal springs to data for 25 precipitation stations in the Alps (IAEA & WMO, 2019). In addition, the data were compared to typical values for water derived from magmatic devolatilization and metamorphic dehydration (Sheppard, 1986; Yardley, 2009). Groundwater circulation temperature was estimated using empirical SiO_2 geothermometer equations (Verma et al., 2008) (Figure S1). We report the minimum, mean and maximum values of these equations. The corresponding circulation depth was calculated by dividing the circulation temperature with the average geothermal gradient in the Alps as described below, following the approach of previous studies (Grasby & Hutcheon, 2001). Note that this calculation assumes that groundwater flow does not affect the geothermal gradient strongly, which may not be true in some cases. The calculated circulation temperatures and depths are minimum estimates, because empirical geothermometer equations do not take into account mixing effects and precipitation of SiO_2 during upward flow (Ferguson et al., 2009). Mixing between shallow and deep sources has been demonstrated for a number of springs in the Alps and may be relatively common (Buser et al., 2013; Sonney et al., 2012; Waber et al., 2017). Geochemical models indicate that maximum circulation temperatures of the deep groundwater component may be double that of bulk samples (Diamond et al., 2018).

The size of the contributing area to each spring was calculated by dividing spring discharge by recharge rate (De Graaf et al., 2015). Note that the recharge rate may vary within the contributing area of each spring and the geometry of these areas is unknown. However, given the relatively low variation (15%) of recharge in watersheds that host the springs (Figure S2), we only used the recharge rate at the spring location for further analyses.

Heat exchange between the subsurface and the groundwater that discharges in springs is given by:

$$H = \rho_f c_f (T_2 - T_1) Q - H_v \qquad \text{(eq. 1)}$$

where H is the heat gain or loss of water (W), ρ_f is the water density (kg m^{-3}), c_f is water specific heat capacity (J kg^{-1} K^{-1}), T_1 and T_2 are groundwater temperature at the start and end of the flow path (K) and Q is groundwater discharge (m^3 a^{-1}). A conceptual model that illustrates flow paths and heat exchange of spring water is included in the supporting information (Figure S3). The term H_v represents the heating of water caused by viscous dissipation, which is often small but can be important in relatively cold springs with a high relief in their contributing area (Manga & Kirchner, 2004). Viscous dissipation is given by:

$$H_v = \rho_f g (h_2 - h_1) Q \qquad \text{(eq. 2)}$$

where h_1 and h_2 are the hydraulic head at the start and the end of the flow path. Note that in contrast to previous work (Manga & Kirchner, 2004) we use the hydraulic head instead of elevation to also take into account the conversion of gravitational potential to elastic energy during subsurface flow.

The net heat exchange with the subsurface is calculated by substituting T_1 by the average recharge temperature T_r (K) and by substituting T_2 by the spring temperature T_s (K) in eq. 1. For the viscous dissipation term, h_1 is substituted by the average elevation of the recharge area z_r (m) and h_2 is substituted by the elevation of the spring, z_s (m). For heat exchange during downward flow we use the average recharge temperature T_r (K) as a value for T_1 and the circulation temperature T_m (K) as the value for T_2 in eq. 1. For the heat exchanged during upward flow T_m is used for T_1 and the spring temperature T_s is used for T_2. For the calculation of the viscous dissipation using eq. 2, h_1 is substituted by z_r and h_2 is substituted by h_m, the hydraulic head at the circulation depth. For the calculation of viscous dissipation during upward flow h_1 is substituted by h_m and h_2 by z_s.

The values of average recharge elevation (z_r) and temperature (T_r) are unknown. However, the bounds of these parameters can be estimated. The maximum elevation was calculated using from the highest elevation in the watershed that the spring was located in, using the Hydrobasin database (Lehner & Grill, 2013) and elevation data (Danielson & Gesch, 2011). The minimum estimate for recharge elevation was equal to the elevation of the spring. Similarly, the minimum and maximum bounds of the recharge temperature were calculated as the recharge temperature at the spring location and the recharge temperature at the highest elevation in the watershed. Recharge temperature was assumed to follow the average annual air temperature (Fick & Hijmans, 2017). Circulation temperature was estimated using the SiO_2 geothermometer as explained above. The hydraulic head at the circulation depth (h_m) is unknown and was chosen as the mean of the spring elevation and the maximum recharge elevation. Note that the uncertainty in h_m only affects viscous dissipation, which is a very small term for most springs.

Temperature and discharge data were not available for all springs in the database. To estimate of the heat flux for all springs, we estimated the discharge for the springs without discharge data, but with temperature data to be equal to the average discharge of the springs with discharge data. Similarly, we estimated the temperature for springs without temperature data as the average of the springs with temperature data.

We compared the heat flux of thermal springs to the background conductive heat flow density in the Alps based on the global heat flow data database (International Heat Flow Commission, 2020), which yielded a mean background heat flow of 76 mW m^{-2}, and a mean geothermal gradient of 26 ˚C km^{-1} (see Text S2 and Figure S3 for more details). The thermal footprint of springs was calculated by dividing the net heat flux of each spring by the mean background heat flow density in the Alps. The net heat flux of springs in the Alps was compared with several mountain belts in North America using a published database of spring heat flow (Ferguson & Grasby, 2011). Note that these values did not take into account viscous dissipation and heat flow may therefore have been slightly overestimated.

4 Results and discussion

The springs are relatively evenly distributed over the Alps, with an average of one spring per 512 km^2 and an average distance between springs of 13 km. The mean temperature of the 364 springs with temperature data is 22 ˚C. The warmest springs are located in northern Italy (Figure 1a), where the La Bollente spring (Bortolami et al., 1983) and Fonte Boiola (Waring & Blankenship, 1965) measured 71 ˚C and 70 ˚C, respectively. The highest discharge rates were observed in the eastern Alps (Figure 1c), where the Fontanon spring in Italy (Cantonati & Spitale, 2009) and the Kroparica spring in Slovenia (Philipp, 2015) discharge at rates of 0.22 m^3 s^{-1} and 0.31 m^3 s^{-1}, respectively. The location, temperature and discharge of thermal springs in the Alps is shown in Figure 1.

The mean discharge of 241 thermal springs is 1.2×10^{-3} m^3 s^{-1}, and total discharge is 2.7 m^3 s^{-1}, which equals a discharge rate of 0.4 mm a^{-1} when spread out evenly over the Alps. This is only 0.08% of the average recharge rate in the Alps of 500 mm a^{-1} (De Graaf et al., 2015). Regarding the 188 springs without discharge data, we assume a mean discharge rate (1.1×10^{-2} m^3 s^{-1}) to estimate the total discharge of approximately 4.4 m^3 a^{-1}, which amounts to 0.7 mm a^{-1} or 0.13% of the total amount of meteoric water that is recharged in the Alps. This relatively low number is roughly in line with published estimates for the Alpine fault in New Zealand where only 0.02% to 0.05% of meteoric water penetrates to depth (Menzies et al., 2016).

All the spring water plots within 1 ‰ $\delta^{18}O$ value of the global meteoric water line and local precipitation values, which indicates a meteoric origin of spring waters (Figure 2a). The compiled SiO_2 concentrations and the calculated values of circulation temperature and depth for 139 of the springs are shown in Figure 2b, 2c and 2d. The circulation temperatures range up to 130 ˚C, which corresponds a depth of 4700 m below the surface based on average conductive geothermal gradients in the Alps (see Text S3, Figure S3). The mean circulation temperature is 64 ˚C, which is equal to a depth of 2100 m below the surface. Note that these depths are minimum estimates due to the limitations of the SiO_2 geothermometer discussed in the Methods. The calculated circulation depths overlap with the depths of upper crustal seismicity in the Alps (Hetényi et al., 2018). This means that fluid pressures changes originating at the surface can be

transferred to seismically active parts of the crust, which given the important role of fluid pressure in fault failure (Hainzl et al., 2006; Hubbert & Rubey, 1959) may affect seismic activity.

The calculated net heat flux of the thermal springs in the Alps is shown in Figure 3. The average net heat flux for thermal springs equals 3.8×10^5 to 6.7×10^5 W. The reported range for spring heat flux and thermal footprint represent endmember (minimum and maximum) uncertainty estimates. The two springs with the highest net heat flux are the Urquelle in Villach, Austria, with a net heat flux of 8.7×10^6 W and Lavey-les-Bains in Switzerland with a net heat flux of 6.5×10^6 W. The calculated net heat flux for 226 springs for which the average temperature and discharge rate are known equals 84 to 151 MW. The net heat flux equals a heat flow density of 0.42 to 0.75 mW m^{-2} when spread out evenly over the Alps. Comparison with the background heat flow density shows that the heat flux by thermal springs is equal to 0.5% to 1.0% of the background heat flux. When the estimated contribution for springs with missing temperature or discharge data is included, the total heat flux of all springs is estimated as 171 to 294 MW. This equals 0.9 to 1.5 mW m^{-2} and is 1.1% to 1.9% of the background conductive heat flux. The thermal footprint of the springs is on average 4.9 to 8.8 km^2 (Figure 3d). This is much larger than the contributing area for each spring, which is on average 0.6 km^2 (Figure 3b), indicating that only a fraction of groundwater recharge discharges at these springs. Viscous dissipation accounts for on average 17% of the total heat output of springs. However, this number is skewed by a small number of low-temperature springs, and the median contribution of viscous dissipation for all springs is 1%.

The net heat flux of the springs is a combination of the cooling of the subsurface by downward groundwater flow, and heating by upward groundwater flow (Figure S1). The cooling by downward groundwater flow for 64 springs with data on circulation temperature is equal to 55 to 97 MW. When the remaining springs are assumed to have the mean value for circulation temperature, the total amount of cooling by all the springs is estimated as 740 to 1264 MW, which equals a heat flow density of 3.7 to 6.2 mW m^{-2} and is 4.8% to 8.3% of the total background heat flow of the Alps. Heating by upward flow for springs with circulation temperature data is calculated as 35 to 65 MW. The heating by all the springs in the database is estimated as 601 to 971 MW, which equals a heat flow density of 3.0 to 4.8 mW m^{-2} and 3.9% to 6.3% of the background heat flow.

Calculation of the discharge and the net hydrothermal heat flux for orogens in North America (Fig. 4) shows that the spring discharge and the heat flux are relatively high. Note that in contrast to the Alps for the other orogens heat flux may be slightly overestimated because viscous dissipation was not taken into account. We hypothesize that the high rate of spring discharge and hydrothermal activity in the Alps may be the result of the Alps being the best explored orogen given its high population density.

The contribution of thermal springs is likely to be only a part of the total amount of deep groundwater flow, because a large part of the deep groundwater may form blind hydrothermal systems without a surface expression, with groundwater discharging diffusely in shallow aquifers, rivers or lakes. Relatively few estimates for the rate of spring versus diffuse discharge have been published. Analysis of Ge/Si ratios in springs and rivers in a basin in the Himalayas showed that diffuse discharge equals 2/3 and 1/3 is discharged in springs (Derry et al., 2009). Similarly, in the Beowawe system in the Basin and Range Province, 2/3 of the total discharge is diffuse discharge (Olmsted & Rush, 1987). For the Alps diffuse discharge is evidenced by

hydrothermal systems without surface expression that have been tapped by tunnels or boreholes. For example, a 75 m long tunnel in Font Salée in the French Alps resulted in discharge with an estimated heat output of 69 MW (Silvestre, 1991) that exceeds any of the natural springs in the Alps. Similarly, in Brigerbad, Switzerland (Buser et al., 2013), and La Léchère, French Alps (Thiébaud et al., 2010), boreholes have tapped artesian groundwater with a higher heat output than existing natural springs.

Deep groundwater flow systems may change location over long timescales due to the competition of permeability increase by fault motion and decrease by mineralization (Woodcock et al., 2007). Although data on this is rare, an example from the Beowawe system documents episodic activation of new flow paths following earthquakes (Howald et al., 2015; Louis et al., 2019). Given that similar processes may operate in many hydrothermal systems this implies that the area affected by hydrothermal activity over longer timescales may be much larger than the area affected by current activity. This may be important for low-temperature thermochronometers that are widely used to quantify the thermal and geological history of mountain belts (Spotila, 2005).

5 Summary and conclusions

We present and analyze a new database of thermal springs in the Alps. Our analyses suggest that thermal springs are fed by meteoric water and the discharge of the springs comprises 0.13% of the total meteoric groundwater budget of the Alps. The circulation depth of the water that discharges in the springs ranges up to 4700 m and has a mean value of 2100 m. This is an underestimate due to the limitations of the SiO_2 geothermometer on which these numbers are based (Ferguson et al., 2009), which means that meteoric groundwater circulates in a substantial part of the upper crust. The circulation depths overlap with the depths of upper crustal seismicity (Hetényi et al., 2018), and therefore meteoric groundwater may play a role in modulating fluid pressure in seismically active faults. In spite of their small contribution to the groundwater budget, the net heat flux by thermal springs accounts for a much higher potion of the total heat budget of the Alps – approximately 1.5%. The net heat flux is a combination of two larger terms: cooling by downward groundwater flow, and heating by upward groundwater flow. Both of these components are two to five times higher than the net heat flux, and probably more due to the underestimation of circulation temperatures. In addition, given that not all deep groundwater flow discharges in thermal springs, the estimates reported here are a minimum estimate for total amount of deep groundwater flow and its contribution to the heat budget.

The average thermal footprint of springs is 6 km^2, which means that on average heat flow and temperatures are affected in an area with a radius of 900 m around active springs, and larger if one assumes that springs do not harvest all the background heat flow over a particular area but harvest a part of the background heat flow over a larger area. Quantifying conductive geothermal gradients and heat flow in mountain belts may be challenging. Although one could avoid using temperature data from areas around active hot springs, these springs may discharge only a part of the overall deep groundwater flow and hydrothermal systems without a surface expression may be common. Moreover, deep groundwater flow systems may change location over long timescales due to permeability changes by fault motion and mineralization and may therefore affect low-temperature thermochronometers even in the absence of a clearly expressed thermal

anomaly. Comparison with orogens in North America shows that the Alps have a relatively high spring discharge and hydrothermal heat flux.

Acknowledgments, Samples, and Data

EL and CvH acknowledge funding by the German Research Foundation (DFG) project 365246344, which is part of the special priority program Mountain Building Process in Four Dimensions. The thermal spring database has been published at Pangaea (submitted, reference to be supplied). The database is also available as supplementary dataset 1 and 2. Data analysis and figures were completed using a set of Jupyter notebooks that are available on GitHub (https://github.com/ElcoLuijendijk/thermal_springs_alps).

References

Bodri, B., & Rybach, L. (1998). Influence of topographically driven convection on heat flow in the Swiss Alps: a model study. *Tectonophysics*, *291*(1–4), 19–27.

Bortolami, G. C., Cravero, M., Olivero, G. F., Ricci, B., & Zuppi, G. M. (1983). Chemical and isotopic measurements of geothermal discharges in the Acqui terme district, Piedmont, Italy. *Geothermics*, *12*(2–3), 185–197. https://doi.org/10.1016/0375-6505(83)90029-9

Buser, M., Eichenberger, U., Jacquod, J., Paris, U., & Vuataz, F. (2013). *Geothermie Brig-Glis, Geothermiebohrungen Brigerbad Phase 2: Schlussbericht Phase 2*.

Cantonati, M., & Spitale, D. (2009). The role of environmental variables in structuring epiphytic and epilithic diatom assemblages in springs and streams of the Dolomiti Bellunesi National Park (south-eastern Alps). *Fundamental and Applied Limnology*, *174*(2), 117–133. https://doi.org/10.1127/1863-9135/2009/0174-0117

Craig, H. (1961). Isotopic variations in meteoric waters. *Science*, *133*(3465), 1702–1703. https://doi.org/10.1126/science.133.3465.1702

Danielson, J. J., & Gesch, D. B. (2011). Global multi-resolution terrain elevation data 2010 (GMTED2010). *US Geol. Surv. Open File Rep*, *1073*, 25.

De Graaf, I. E. M., Sutanudjaja, E. H., Van Beek, L. P. H., & Bierkens, M. F. P. (2015). A high-resolution global-scale groundwater model. *Hydrology and Earth System Sciences*, *19*(2), 823–837. https://doi.org/10.5194/hess-19-823-2015

Dempster, T. J., & Persano, C. (2006). Low-temperature thermochronology: Resolving geotherm shapes or denudation histories? *Geology*, *34*(2), 73–76. https://doi.org/10.1130/G21980.1

Derry, L. A., Evans, M. J., Darling, R., & France-Lanord, C. (2009). Hydrothermal heat flow near the Main Central thrust, central Nepal Himalaya. *Earth and Planetary Science Letters*, *286*(1), 101–109.

Diamond, L. W., Wanner, C., & Waber, H. N. (2018). Penetration depth of meteoric water in orogenic geothermal systems. *Geology*, *46*(12), 1083–1066. https://doi.org/10.1130/G45394.1

Duddy, I. R., Green, P. F., Bray, R. J., & Hegarty, K. A. (1994). Recognition of the thermal

effects of fluid flow in sedimentary basins. *Geological Society, London, Special Publications*, *78*(1), 325–345.

Ferguson, G., & Grasby, S. E. (2011). Thermal springs and heat flow in North America. *Geofluids*, *11*(3), 294–301. https://doi.org/10.1111/j.1468-8123.2011.00339.x

Ferguson, G., Grasby, S. E., & Hindle, S. R. (2009). What do aqueous geothermometers really tell us? *Geofluids*, *9*(1), 39–48. https://doi.org/10.1111/j.1468-8123.2008.00237.x

Ferguson, G., Mcintosh, Jj. C., Grasby, S. E., Hendry, M. J., Lindsay, M. B. J., Jasechko, S., & Luijendijk, E. (2018). The Persistence of Brines in Sedimentary Basins. *Geophysical Research Letters*, *45*, 4851–4858. https://doi.org/10.1029/2018GL078409

Fick, S. E., & Hijmans, R. J. (2017). WorldClim 2: new 1-km spatial resolution climate surfaces for global land areas. *International Journal of Climatology*, *37*(12), 4302–4315.

Forster, C., & Smith, L. (1989). The Influence of Groundwater Flow on Thermal Regimes in Mountainous Terrain: A Model Study. *Journal of Geophysical Research*, *94*(B7), 9439–9451. https://doi.org/10.1029/JB094iB07p09439

Fukutomi, T. (1970). Order of magnitude for total discharge-rate of heat energy from all of the hot spring localities in Japan. *Geophysical Bulletin of the Hokkaido University*, *23*, 9–13. https://doi.org/10.14943/gbhu.23.9

Gleeson, T., Befus, K. M., Jasechko, S., Luijendijk, E., & Cardenas, M. B. (2016). The global volume and distribution of modern groundwater. *Nature Geoscience*, *9*(2), 161–167. https://doi.org/10.1038/ngeo2590

Grasby, S. E., & Hutcheon, I. (2001). Controls on the distribution of thermal springs in the southern Canadian Cordillera. *Canadian Journal of Earth Sciences*, *38*(3), 427–440. https://doi.org/10.1139/e00-091

Hainzl, S., Kraft, T., Wassermann, J., Igel, H., & Schmedes, E. (2006). Evidence for rainfall-triggered earthquake activity. *Geophysical Research Letters*, *33*(19), 1–5. https://doi.org/10.1029/2006GL027642

Handy, M. R., M. Schmid, S., Bousquet, R., Kissling, E., & Bernoulli, D. (2010). Reconciling plate-tectonic reconstructions of Alpine Tethys with the geological-geophysical record of spreading and subduction in the Alps. *Earth-Science Reviews*, *102*(3–4), 121–158. https://doi.org/10.1016/j.earscirev.2010.06.002

Hetényi, G., Epard, J. L., Colavitti, L., Hirzel, A. H., Kiss, D., Petri, B., Scarponi, M., Schmalholz, S. M., & Subedi, S. (2018). Spatial relation of surface faults and crustal seismicity: a first comparison in the region of Switzerland. *Acta Geodaetica et Geophysica*, *53*(3), 439–461. https://doi.org/10.1007/s40328-018-0229-9

Hoke, L., Poreda, R., Reay, A., & Weaver, S. D. (2000). The subcontinental mantle beneath southern New Zealand, characterised by helium isotopes in intraplate basalts and gas-rich springs. *Geochimica et Cosmochimica Acta*, *64*(14), 2489–2507. https://doi.org/10.1016/S0016-7037(00)00346-X

Howald, T., Person, M., Campbell, A., Lueth, V., Hofstra, A., Sweetkind, D., Gable, C. W., Banerjee, A., Luijendijk, E., Crossey, L., Karlstrom, K., Kelley, S., & Phillips, F. M. (2015). Evidence for long timescale (>103 years) changes in hydrothermal activity induced

by seismic events. *Geofluids*, *15*(1–2), 252–268. https://doi.org/10.1111/gfl.12113

Hubbert, M. K., & Rubey, W. W. (1959). Role of fluid pressure in mechanics of overthrust faulting: I. Mechanics of fluid-filled porous solids and its application to overthrust faulting. *Bulletin of the Geological Society of America*, *70*(2), 115–166. https://doi.org/10.1130/0016-7606(1959)70[115:ROFPIM]2.0.CO;2

IAEA, & WMO. (2019). *Global Network of Isotopes in Precipitation: The GNIP Database*.

Ingebritsen, S. E., Sherrod, D. R., & Mariner, R. H. (1992). Rates and patterns of groundwater flow in the Cascade Range volcanic arc, and the effect on subsurface temperatures. *Journal of Geophysical Research*, *97*(B4), 4–599.

International Heat Flow Commission. (2020). *Global heat flow database*.

Jasechko, S., Perrone, D., Befus, K. M., Bayani Cardenas, M., Ferguson, G., Gleeson, T., Luijendijk, E., McDonnell, J. J., Taylor, R. G., Wada, Y., & Kirchner, J. W. (2017). Global aquifers dominated by fossil groundwaters but wells vulnerable to modern contamination. *Nature Geoscience*, *10*(6), 425–429. https://doi.org/10.1038/ngeo2943

Karlstrom, K. E., Crossey, L. J., Hilton, D. R., & Barry, P. H. (2013). Mantle 3He and CO2 degassing in carbonic and geothermal springs of Colorado and implications for neotectonics of the Rocky Mountains. *Geology*, *41*(4), 495–498.

Lehner, B., & Grill, G. (2013). Global river hydrography and network routing: baseline data and new approaches to study the world's large river systems. *Hydrological Processes*, *27*(15), 2171–2186.

Louis, S., Luijendijk, E., Dunkl, I., & Person, M. (2019). Episodic fluid flow in an active fault. *Geology*, *47*(10), 938–942. https://doi.org/10.1130/G46254.1

Luijendijk, E. (2019). Beo v1.0: Numerical model of heat flow and low-temperature thermochronology in hydrothermal systems. *Geoscientific Model Development*, *12*, 4061–4073. https://doi.org/10.5194/gmd-12-4061-2019

Manga, M. (2001). Using springs to study groundwater flow and active geological processes. *Annual Review of Earth and Planetary Sciences*, *29*, 201–228. https://doi.org/10.1016/S0950-1401(10)04008-5

Manga, M., & Kirchner, J. W. (2004). Interpreting the temperature of water at cold springs and the importance of gravitational potential energy. *Water Resources Research*, *40*(5), 1–8. https://doi.org/10.1029/2003WR002905

Manning, A. H., & Caine, J. S. (2007). Groundwater noble gas, age, and temperature signatures in an Alpine watershed: Valuable tools in conceptual model development. *Water Resources Research*, *43*(4). https://doi.org/10.1029/2006WR005349

Maréchal, J.-C., Perrochet, P., & Tacher, L. (1999). Long-term simulations of thermal and hydraulic characteristics in a mountain massif: The Mont Blanc case study, French and Italian Alps. *Hydrogeology Journal*, *7*(4), 341–354.

Menzies, C. D., Teagle, D. A. H., Niedermann, S., Cox, S. C., Craw, D., Zimmer, M., Cooper, M. J., & Erzinger, J. (2016). The fluid budget of a continental plate boundary fault: Quantification from the Alpine Fault, New Zealand. *Earth and Planetary Science Letters*,

445, 125–135. https://doi.org/10.1016/j.epsl.2016.03.046

Olmsted, F. H., & Rush, F. E. (1987). Hydrogeologic Reconnaissance of the Beowawe Geysers Geothermal Area , Nevada. *Geothermics*, *16*(1), 27–46.

Pedersen, K. (1993). The deep subterranean biosphere. *Earth Science Reviews*, *34*(4), 243–260. https://doi.org/10.1016/0012-8252(93)90058-F

Person, M., Mulch, A., Teyssier, C., & Gao, Y. (2007). Isotope transport and exchange within metamorphic core complexes. *American Journal of Science*, *307*(3), 555–589.

Philipp, S. (2015). *Hydrochemistry and Isotopic Analysis of Deep (Partly Thermal) Wells and Springs in NW-Slovenia*. Technische Universität.

Poulet, T., Veveakis, M., Herwegh, M., Buckingham, T., & Regenauer-lieb, K. (2014). Modeling episodic fluid-release events in the ductile carbonates of the Glarus thrust. *Geophys. Res. Lett*, 7121–7128. https://doi.org/10.1002/2014GL061715.Received

Schmid, S. M., Fügenschuh, B., Kissling, E., & Schuster, R. (2004). Tectonic map and overall architecture of the Alpine orogen. *Eclogae Geologicae Helvetiae*, *97*(1), 93–117. https://doi.org/10.1007/s00015-004-1113-x

Sheppard, S. M. F. (1986). Characterization and isotopic variations in natural waters. *Reviews in Mineralogy*, *16*, 165–184. https://doi.org/10.2138/rmg.1985.16.6

Silvestre, J. P. (1991). Thermalisme et minéralisme - Le thermalisme dans les Hautes Alpes Rapport final. In *Rapport BRGM: Vol. R 33971 PA*.

Sonney, R., Vuataz, F. D., & Schill, E. (2012). Hydrothermal circulation systems of the Lavey-les-Bains, Saint-Gervais-les-Bains and Val d'llliez areas associated with the Aiguilles Rouges Massif in Switzerland and France. In *Bulletin fuer Angewandte Geologie* (Vol. 17, Issue 1, pp. 29–47).

Spotila, J. A. (2005). Applications of low-temperature thermochronometry to quantification of recent exhumation in mountain belts. *Reviews in Mineralogy and Geochemistry*, *58*(1), 449.

Sumi, K. (1980). Relationship between the distributions of the Quatemary volcanoes and the rate of heat discharge by hot water in Japan. *Bulletin of the Geological Survey of Japan*, *31*(6), 255–266.

Thiébaud, E., Dzikowski, M., Gasquet, D., & Renac, C. (2010). Reconstruction of groundwater flows and chemical water evolution in an amagmatic hydrothermal system (La Léchère, French Alps). *Journal of Hydrology*, *381*(3–4), 189–202. https://doi.org/10.1016/j.jhydrol.2009.11.041

Umeda, K., Sakagawa, Y., Ninomiya, A., & Asamori, K. (2007). Relationship between helium isotopes and heat flux from hot springs in a non-volcanic region, Kii Peninsula, southwest Japan. *Geophysical Research Letters*, *34*(5), 1–5. https://doi.org/10.1029/2006GL028975

Verma, S. P., Pandarinath, K., & Santoyo, E. (2008). SolGeo: A new computer program for solute geothermometers and its application to Mexican geothermal fields. *Geothermics*, *37*(6), 597–621. https://doi.org/10.1016/j.geothermics.2008.07.004

Waber, H. N., Schneeberger, R., Mäder, U. K., & Wanner, C. (2017). Constraints on Evolution and Residence time of Geothermal Water in Granitic Rocks at Grimsel (Switzerland).

Procedia Earth and Planetary Science, *17*(February), 774–777. https://doi.org/10.1016/j.proeps.2017.01.026

Walvoord, M. A., Pegram, P., Phillips, F. M., Person, M., Kieft, T. L., Fredrickson, J. K., McKinley, J. P., & Swenson, J. B. (1999). Groundwater flow and geochemistry in the Southeastern San Juan Basin: Implications for microbial transport and activity. *Water Resour. Res.*, *35*(5), 1409–1424. https://doi.org/10.1029/1999WR900017

Waring, G. A., & Blankenship, R. R. (1965). *Thermal Springs of the United States and Other Countries: A Summary* (Vol. 492). US Government Printing Office.

Whipp, D. M., & Ehlers, T. A. (2007). Influence of groundwater flow on thermochronometer-derived exhumation rates in the central Nepalese Himalaya. *Geology*, *35*(9), 851–854.

Wintsch, R. P., Christoffersen, R., & Kronenberg, A. K. (1995). Fluid-rock reaction weakening of fault zones. *J. Geophys. Res.*, *100*(B7), 13021–13032. https://doi.org/10.1029/94JB02622

Woodcock, N. H., Dickson, J. A. D., & Tarasewicz, J. P. T. (2007). Transient permeability and reseal hardening in fault zones: evidence from dilation breccia textures. *Geological Society, London, Special Publications*, *270*(1), 43–53. https://doi.org/10.1144/gsl.sp.2007.270.01.03

Yardley, B. W. D. (2009). The role of water in the evolution of the continental crust. *Journal of the Geological Society*, *166*(4), 585–600. https://doi.org/10.1144/0016-76492008-101

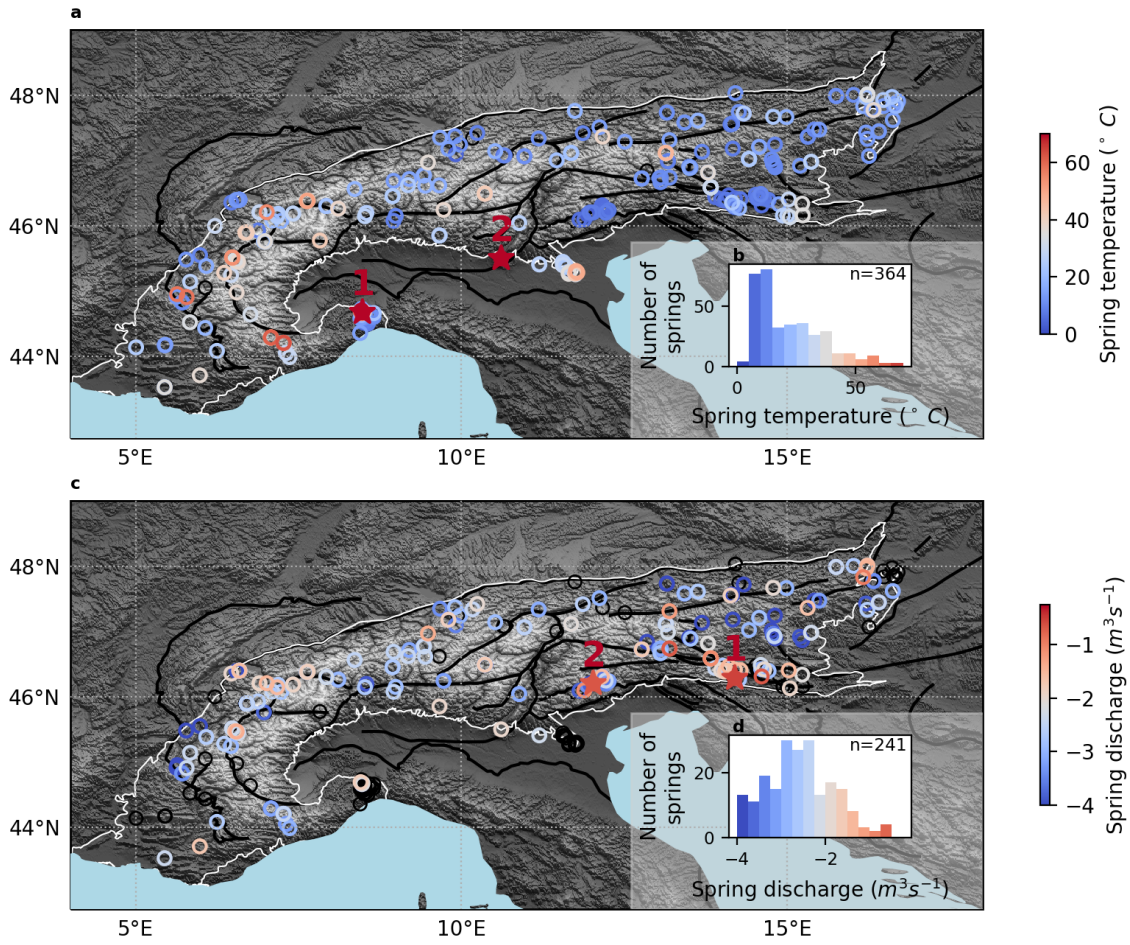

Figure 1. The location, temperature and discharge of thermal springs in the Alps. Panel a and c show maps of the temperature and discharge of thermal springs, respectively. Panel b and d show histograms of the temperature and discharge of thermal springs. The red numbers show the location of the two springs with the highest temperature (panel a) and discharge (panel c). Black circles denote springs without temperature or discharge data. The outline of the Alps is shown in white, and major fault zones are shown by black lines (Handy et al., 2010; Schmid et al., 2004).

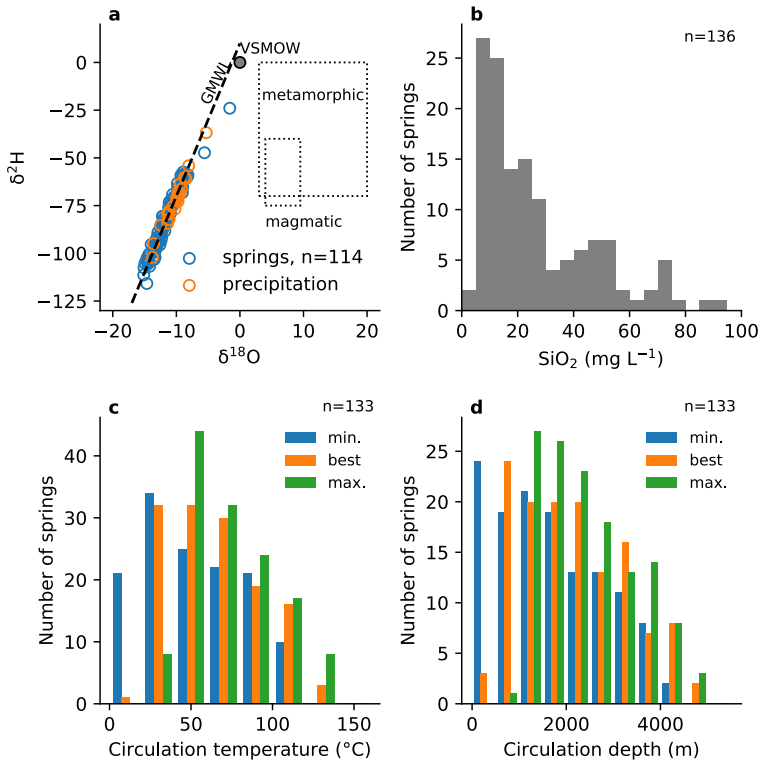

Figure 2. Source, circulation temperature and circulation depth of thermal spring water. (a) Comparison between δ^2H and $\delta^{18}O$ in spring water and in precipitation in the Alps and typical values for water derived from metamorphic and magmatic sources (Yardley, 2009). VSMOW denotes Vienna Standard Mean Ocean Water, GMWL denotes the global meteoric water line (Craig, 1961), (b) SiO_2 concentration in thermal springs, (c) Calculated circulation temperature and (d) circulation depth. Circulation depth was calculated using the circulation temperature and an average geothermal gradient of 26 ˚C km^{-1}. The min., max. and best values in panel c and d represent the circulation temperature and depth using the lowest, highest and mean value of the geothermometer equations, respectively. Note that for three springs the SiO_2 value was lower than 5 mg L-1, which is the lower limit for which the geothermometer equations are valid.

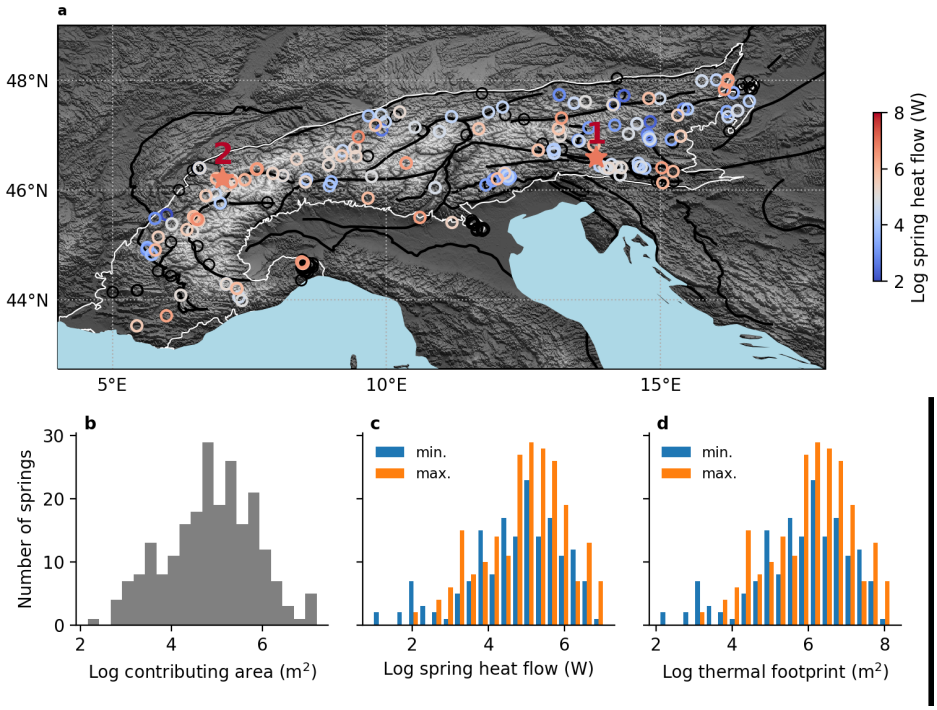

Figure 3. Calculated net heat flux, contributing area and thermal footprint for thermal springs in the Alps. Panel a shows a map of the best estimate spring heat flow, which is the mean of the minimum and maximum estimates discussed in the text. Black circles denote springs without temperature or discharge data. The outline of the Alps is shown in white, and major fault zones are shown by black lines (Handy et al., 2010; Schmid et al., 2004). Red numbers show the location of the two springs with the highest net heat flux. Panel b, c and d show histograms of the calculated contributing area, net heat flow and thermal footprint of the springs, respectively. Panel c and d show min. and max. values that represent uncertainty ranges as discussed in the text. Note that we did not calculate an uncertainty range for contributing area.

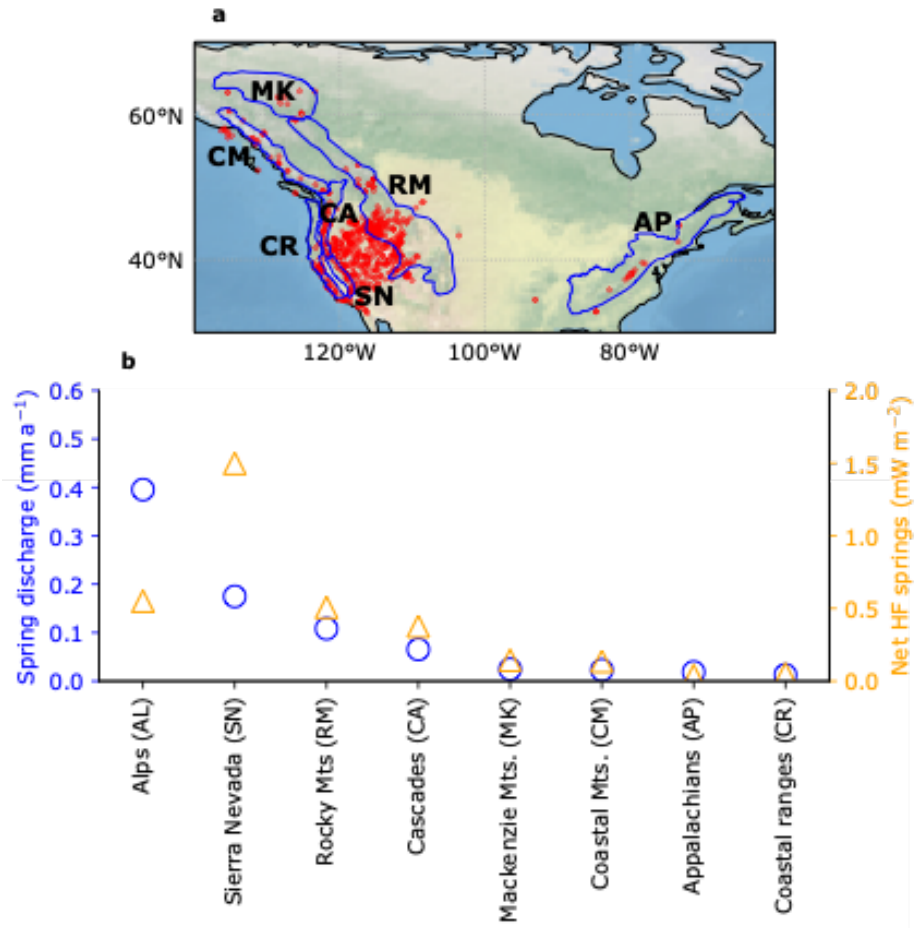

Figure 4. Comparison of thermal spring discharge and net heat flux by thermal springs in the Alps and number of orogens in North America. Panel a shows the locations of the orogens in north America. Thermal springs are indicated by red dots. Panel b shows the aerially averaged discharge and net heat flux density of thermal springs for the Alps and the North American orogens. Note that the values are the discharge and heat flux of springs with discharge and temperature data, the heat flux estimate for the Alps that includes springs with missing temperature or discharge data was not included here.

Geophysical Research Letters

Supporting Information for

Using thermal springs to quantify deep groundwater flow and its thermal footprint in the Alps and North American orogens

Elco Luijendijk[1], Theis Winter[1,2], Saskia Köhler[1,3], Grant Ferguson[4], Christoph von Hagke[5], Jacek Scibek[6]

[1]Department of structural geology & geodynamics, University of Göttingen, Goldschmidtstrasse 3, 37077, Göttingen, Germany

[2]Chair of Hydrogeology, Faculty of Civil, Geo and Environmental Engineering, Technical University of Munich, Arcisstr. 21, 80333 Munich, Germany

[3]GeoZentrum Nordbayern, Universität Erlangen-Nürnberg, Schlossgarten 5, 91054 Erlangen, Germany

[4]Department of Civil, Geological and Environmental Engineering, University of Saskatchewan, 57 Campus Drive, Saskatoon, Canada

[5]Geological Institute of the RWTH Aachen University, Wüllnerstr. 2, 52056 Aachen, Germany.

[6]No fixed address at present (travelling through Japan)]

Contents of this file

Introduction

The supporting information presented here provides more detail for the data compilation effort that led to the thermal spring database of the Alps (Text S1) and the calculation of the conductive background geothermal gradient and heat flow of the Alps (Text S2). In addition, the document includes six supporting figures that are cited in the main text and one supporting table that details the number and type of data included in the thermal spring database.

Text S1: Thermal spring database.

The thermal spring database is based on several existing databases, including a global database (Waring & Blankenship, 1965) and a regional database for Switzerland (Sonney & Vuataz, 2008). In addition, a large amount of data was obtained from published literature and technical reports. More details on the data sources for each spring are included in the database (DOI to Pangaea dataset to be supplied)

The boundary of the Alps was based on published geological maps (Handy et al., 2010; Schmid et al., 2004). In addition to springs within the Alps, we included springs that were at a distance of up to 0.1 degree (approx. 10 km) or less from the Alps, because these springs are likely to be driven by the high recharge and hydraulic gradients in the Alps.

Our objective was to only include natural springs. A number of natural springs have over time been tapped by shallow wells but are still referred to in the literature as springs. We included springs with shallow wells in the database and used a cutoff of 100 m to distinguish shallow and deep wells. The cutoff of 100 m was chosen such temperature of the water that discharges in these wells is not affected significantly by the increased background temperature at the depths at which these springs are tapped. Given the geothermal gradient is approximately 3 ˚C higher at a depth of 100 m. Overall 32 of the 394 springs in the database consist of shallow wells, the remainder were natural springs. The distribution of the values of discharge and temperatures for these springs for discharge and temperature are similar to the distribution for the springs without wells (Figure S6). Therefore, including the springs tapped by shallow wells did not introduce a bias in our analysis.

Text S2: Calculation of background geothermal gradients and heat flow.

We compared the heat flux of thermal springs to the background conductive heat flow density in the Alps based on the global heat flow data database (International Heat Flow Commission, 2020) (Figure S4). The database consists of 181 datapoints with data on heat flow density and 19 points with data on geothermal gradients. With the area of the Alps of 202×10^3 km^2 there is on average one heat flow datapoint per 1117 km^2, and the average distance between datapoints is 19 km. Note that for the calculation of the average geothermal gradient data from measurements in lake sediments were omitted, because these may not be representative of the deeper parts of the upper crust. The mean background heat flow is 76 mW m^{-2}, and the mean geothermal gradient is 26 ˚C km^{-1}. Given the high variation in background heat flow at small spatial scales (Figure S4) no further attempt was made to interpolate heat flow density, and the mean heat flow density value was used for further analysis. The thermal footprint of springs was calculated by dividing the net heat flux of each spring by the mean background heat flow density in the Alps.

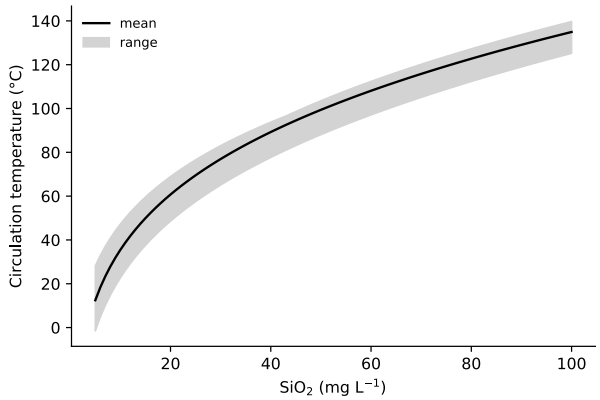

Figure S1 Theoretical relation between SiO2 concentration and minimum circulation temperature using a range of 9 geothermometer equations (Verma et al., 2008). The mean value represents the mean of the 9 different geothermometer equations

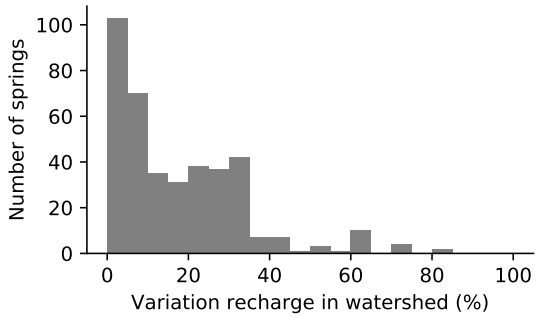

Figure S2. Variation of groundwater recharge in watersheds that host thermal springs. The variation was calculated as the difference between the minimum and maximum value divided by the maximum value.

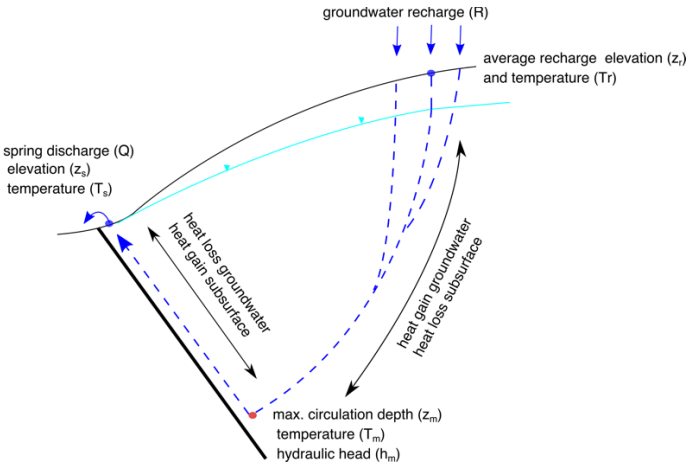

Figure S3. Conceptual model of the flow paths of groundwater that discharges in thermal springs and heat exchange between groundwater and the subsurface.

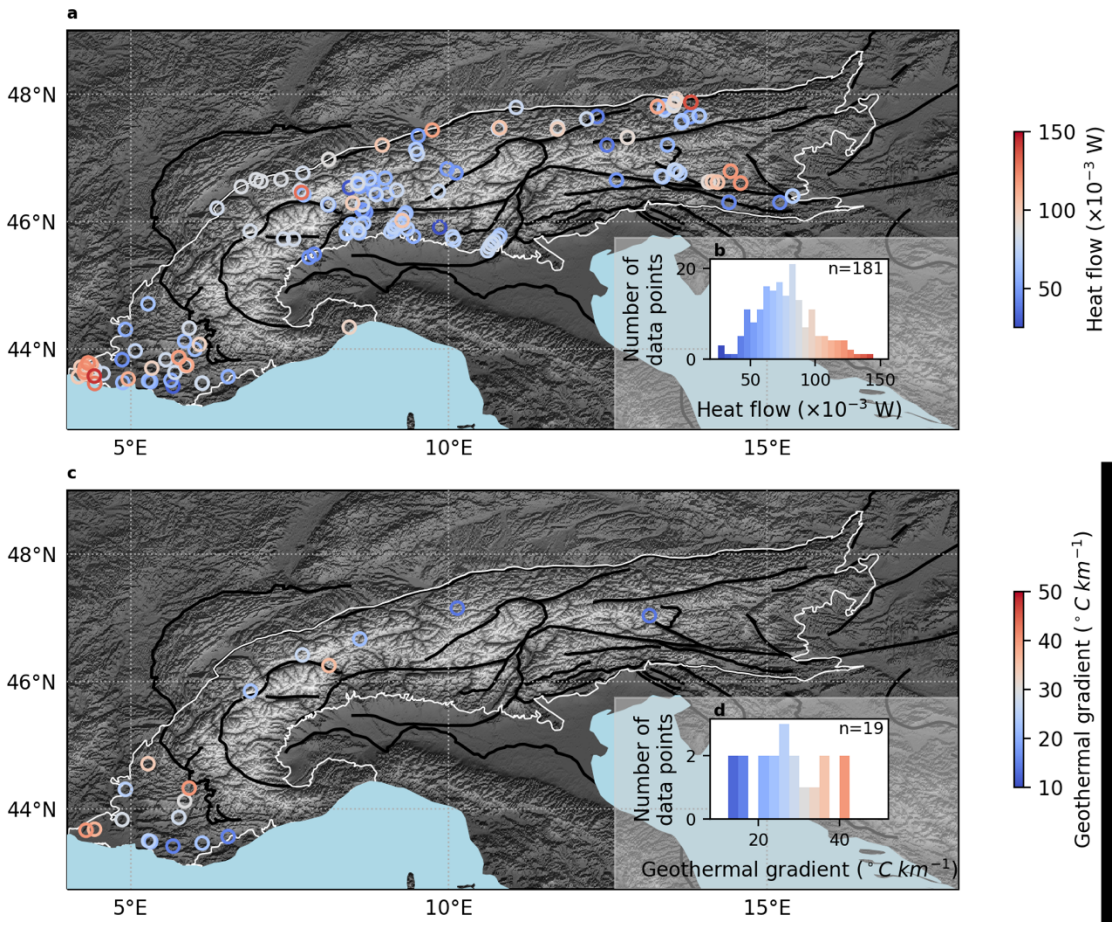

Figure S4. Map of the background heat flow and geothermal gradient in the Alps. Panel a and b show heat flow and panel c and d show geothermal gradients. The data are based on the global heat flow database (International Heat Flow Commission, 2020). The outline of the Alps is shown in white, and major fault zones are shown by black lines (Handy et al., 2010; Schmid et al., 2004). Note that the map of geothermal gradient only contains data from boreholes, tunnels and mines. Data from measurements in lake bottom sediments were omitted.

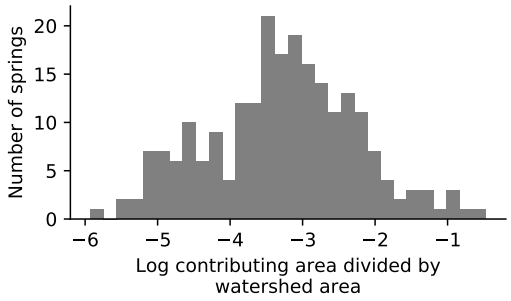

Figure S5. Comparison of the calculated contributing area of each spring with the area of the watershed that each spring is located in.

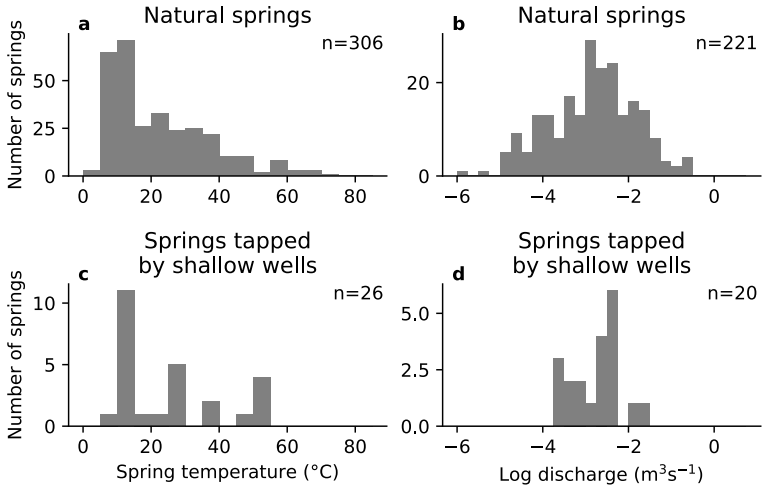

Figure S6. Comparison of temperature and discharge for natural springs and springs tapped by shallow (<100 m) wells.

Type of data	**Number of springs**
Temperature	364
Discharge	241
Temperature and discharge	226
Temperature or discharge	379
^{18}O	127
^{2}H	115
SiO_2	136
Total number of springs	**394**

Table S1. Type of data available in the thermal spring database (reference to Pangaea to be supplied once publication of dataset is complete).